Published in International Journal of Fatigue Vol. 31 (2009) p. 250–262, http://dx.doi.org/10.1016/j.ijfatigue.2008.09.002

Introduction of a Fretting-Fatigue Mapping concept: Development of a dual crack nucleation – crack propagation approach to formalize Fretting Fatigue damage

S. Fouvry, K.J. Kubiak
LTDS, CNRS, Ecole Centrale de Lyon, Ecully 69134 Cedex, France
krzysztof@kubiak.co.uk

Abstract

Fretting fatigue induced by combined localized cyclic contact motion and external bulk fatigue loadings may result in premature and dramatic failure of the contacting components. Depending on fretting and fatigue loading conditions, crack nucleation and possibly crack propagation can be activated. This paper proposes a procedure for estimating these two damage thresholds. The crack nucleation boundary is formalized by applying the Crossland high cycle fatigue criterion taking into account the stress gradient and the ensuing "size effect". The prediction of the crack propagation condition is formalized using a short crack arrest description. Applied to a AISI 1034 steel, this methodology allows the development of an original Material Response Fretting Fatigue Map (FFM), where the different material responses related to crack nucleation, crack arrest and catastrophic failure are established and formalized.

Keywords: Fretting Fatigue, Crack nucleation, Crack arrest, AISI 1034 steel, Ti-6Al-4V, Fretting palliatives.

1. Introduction

Fretting is a small amplitude oscillatory movement, which may occur between contacting surfaces that are subjected to vibration or cyclic stress. Combined with cyclic bulk fatigue loading, the so-called fretting-fatigue loading can induce catastrophic cracking phenomena which critically reduce the endurance of assemblies. Considered to be a plague for modern industry, fretting-fatigue is encountered in all quasi-static contact loadings subjected to vibration and cyclic fatigue and thus concerns many industrial branches (helicopters, aircraft, trains, ships, trucks, ….) [1, 3].

As illustrated in Figure 1, fretting fatigue loading can be characterized by the superposition of a heterogeneous cyclic stress gradient related to the contact loading and a homogeneous fatigue bulk loading.

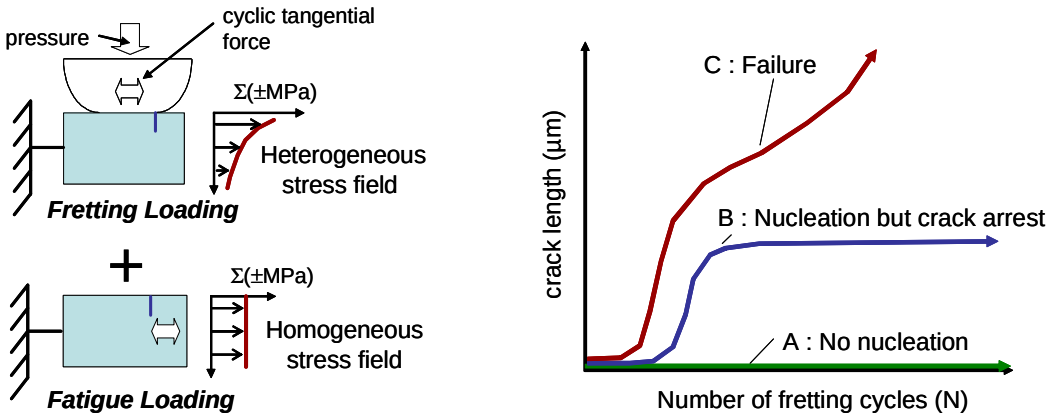

Fig. 1: Illustration of the Fretting Fatigue phenomenon: (a) Schematic of the combined contact and bulk stress (NB: fatigue and contact loading are usually coupled and a function of the assembly stiffness); (b) Illustration of the different cracking damage evolutions which can be observed under fretting loading conditions.

Indeed, the contact stress decreases asymptotically below the interface. From this typical stress distribution, cracking damage will evolve in three different ways. Below a threshold fretting fatigue condition, no cracks are nucleated and the system runs under safe crack nucleation condition. Above this threshold, two evolutions can be observed: for intermediate loading conditions, a crack will nucleate, however, due to the very sharp decrease of the contact stress below the interface, it will finally stop. This typical behavior defines the safe crack arrest domain [3]. Imposing higher contact and/or bulk fatigue loadings, the nucleated crack cannot stop and will propagate until final failure is reached. This defines the ultimate failure domain.

During the past decades, a significant effort has been made both to formalize the crack nucleation and the crack arrest conditions. The crack nucleation phenomenon is commonly addressed by transposing conventional multiaxial fatigue criteria [4, 5]. Specific analysis has been devoted to formalize the contact stress gradient effects (i.e contact size effect). Different approaches like determining an averaged stress state over a representative process volume [6, 7] but also “notch stress” similitude approaches have been developed [8, 9]. The crack arrest description has been formalized by computing the evolution of the stress intensity factor

below the interface, and by predicting the crack arrest condition using short crack arrest formalisms derived from Kitagawa and El Haddad models [10-12].

The objective of this work is to combine these two approaches in order to describe the different fretting fatigue damage through the synthetic form of a Fretting Fatigue mapping concept (Fig. 2). The three damage behaviors are reported as a function of the fretting loading (Y axis) and the fatigue loading (X axis).

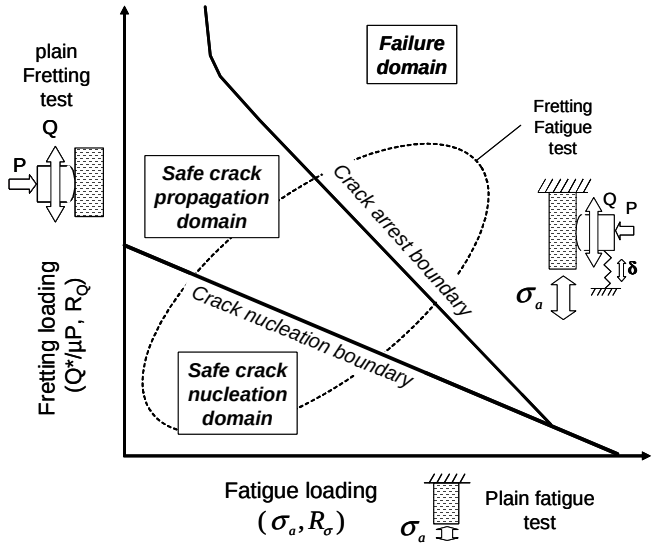

Fig. 2 : Illustration of the Fretting-Fatigue Mapping concept defined for partial slip condition.

Then the plain fatigue parameter along the X axis will be determined from conventional fatigue tests whereas the plain fretting damage along the Y axis will be identified from plain fretting, also called fretting wear test condition. Note that if crack nucleation and crack propagation can be identified when a fatigue loading is imposed, only crack nucleation can be assessed under a pure fretting configuration. Indeed, the contact loading can nucleate the crack but cannot propagate it until failure. Finally, the combined fretting-fatigue test will permits to identify respectively the crack nucleation and crack arrest boundaries in the intermediate domains. This mapping description provides a synthetic overview of fretting fatigue damage. To be effective it nevertheless requires an explicit description of loading parameters (i.e. the loading variables defining the fatigue (X) and fretting (Y) axes). The first step is to relate the fatigue loading to the fatigue stress amplitude normalized by the fatigue limit (σ_a/σ_d). Defining the fretting loading parameter is not so easy. This variable must be representative of the cyclic contact loading, and sufficiently useful for an experimental application. Due to its dominating influence on cyclic stressing, the tangential force amplitude

(Q*) is first considered. The analysis is restricted to the partial slip domain and therefore it is normalized by the value at the sliding transition (i.e. $Q^*/\mu P$). Like for any fatigue problem, the mean stress level plays a critical role in the damage evolution. Both fretting and fatigue loadings have therefore been related to the corresponding stress ratii R_Q and R_s respectively. To avoid any perturbation induced by this latter aspect, this investigation is developed for pure alternated stress conditions (i.e. $R=R_Q=R_s=-1$). Introducing this new mapping concept, the present investigation develops a combined experimental and modeling methodology to identify the damage boundaries and to provide an explicit description of the various types of fretting-fatigue damage.

2. Experimental conditions

2.1. Materials

The fretting fatigue phenomena involve numerous complex mechanisms, which is why, to establish a predictive methodology, the investigation must be calibrated on a well known material. The material used for the experimental investigation and the construction of the model is a low carbon steel alloy, AISI 1034. Fully investigated by Gros [13], it displays a ferrite-perlite structure with the mechanical and fatigue properties listed in Table 1. In order to compare the influence of the material, the Fretting-Fatigue response of a representative Ti-6Al-4V alloy is computed, applying a similar methodology. Chromium 52100 steel was chosen for the cylindrical counterbody in order to ensure elastically similar conditions whilst simultaneously ensuring that cracks arose only in the plane specimens.

Table 1 : Mechanical properties of the materials

Materials	AISI 1034 [13] (plane)	Ti-6Al-4V [14, 15] (plane)	52100 (cylinder)
Young's modulus E (GPa)	200	119	210
Poisson's coefficient ν	0.3	0.33	0.3
Yield stress σ_Y (0.2%) (MPa)	350	890	1700
Ultimate stress σ_{UTS} (MPa)	600	970	2000
Bending Fatigue limit σ_d (MPa) (R=-1, 10^7 cycles)	270 ± 10	450± 10	-
Shear fatigue limit τ_d (MPa) (R=-1, 10^7 cycles)	170 ± 10	260 ± 10	-
long crack threshold ΔK_0 (R=-1) (MPa$\sqrt{m}$)	7 ± 1	5± 1	-
Long crack length transition b_0 (µm)	170	31	-

2.1. Contact configurations

A similar 2D cylinder/plane configuration was chosen both for plain fretting and fretting fatigue test experiments. The radius of the 52100 steel cylinder is R = 40 mm and the pad length L = 6 mm, giving plane strain conditions near the central axis of the fretting scar . Both AISI 1034 planes and fatigue specimens used respectively for plain fretting and fretting fatigue tests display a T=12 mm thickness. The normal load is fixed at $P=F_n/L= 227$ N/mm inducing a maximum Hertzian pressure of p_{0H} = 450 MPa and a Hertzian contact half-width of a_H= 320 µm. In order to minimize edge-effects, the contact pad thickness and the transverse width of the plane specimen were machined to the same size. Hence, whilst the side faces of the contact are traction-free, approximately plane-strain conditions are present along the centerline of the contact. This means that the pressure distribution decreases from a maximum value along the central region to a lower value towards the contact ends, and eliminates any stress singularity problems [16]. Finally, the surfaces in contact were carefully polished to a mirror state (R_a around 0.05 µm).

2.3. Test conditions

As illustrated in Figure 3, two different test apparatuses were involved to quantify respectively the fretting and the fatigue influences in cracking processes.

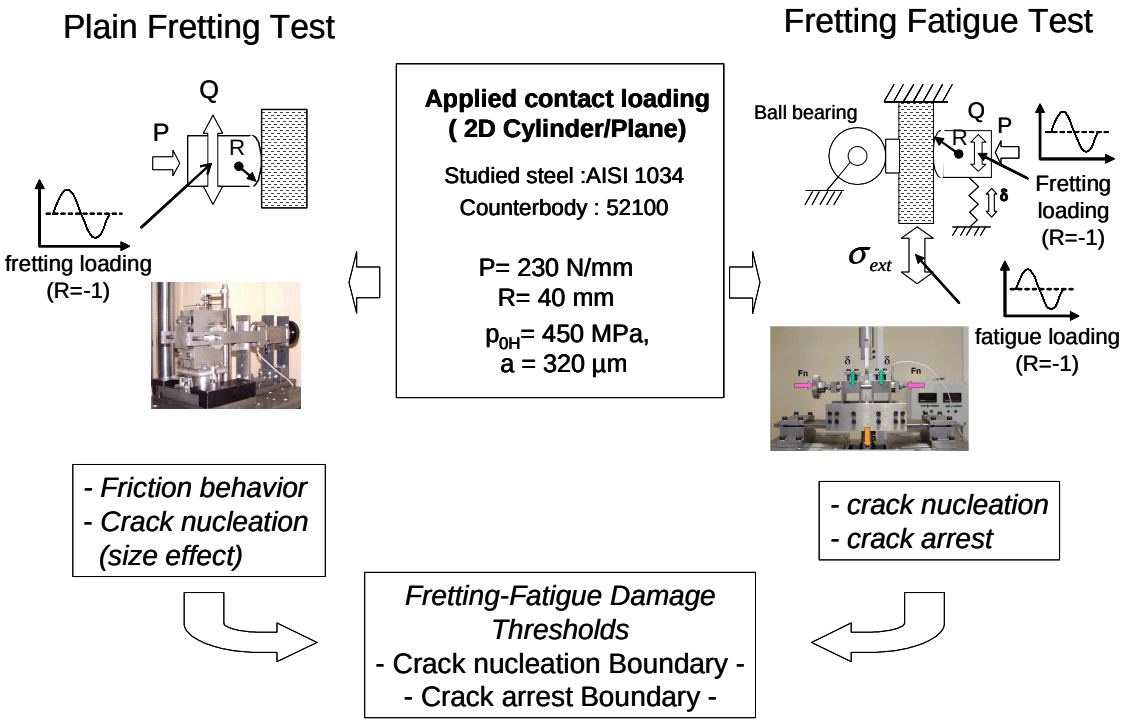

Fig. 3 : Illustration of the experimental strategy applied to identify the tribological properties, the crack nucleation and crack arrest conditions under plain fretting and fretting-fatigue loading conditions.

Plain fretting test

The plain fretting stress conditions were achieved on a dedicated fretting wear test [17]. Fretting was applied by imposing a nominally static normal force (F_n= P.L), followed by a purely alternating cyclic displacement amplitude ($\delta*$), so that an alternating cyclic tangential load (F_t=Q*.L) was generated on the contact surface. During a test, F_n, F_t and δ were recorded, from which the δ - F_t fretting loop can be plotted; this cycle is characterized respectively by the tangential force (F_t) and slip displacement (δ*) amplitude. By analyzing the fretting loop, the sliding condition can be identified and the loading condition adjusted if necessary to maintain a partial slip contact configuration.

Fretting Fatigue test

The fretting fatigue apparatus is based on the conventional principle first introduced by the Oxford group [3] and successively developed by other research teams [5]. It consists of a hydraulic actuator imposing a fatigue loading on a fatigue specimen. A cylinder pad is applied on one side of the fatigue specimen. Hence, the contact loading is induced by the relative displacement between the fatigue specimen and the pad at the contact point. By adjusting the pad holder stiffness and/or the position of the contact along the fatigue specimen, it is possible to control the contact tangential loading with regards to the applied bulk stress. The tangential loading is determined either by strain gauges fixed on the pad holder apparatus or by differential force measurements at each side of the fatigue specimen. Compared to classical setups, the LTDS system displays the following improvements [18]:

- A laser extensometer is adapted to measure the relative displacement between the pad and the fatigue specimen at the contact point. It allows the fretting loop to be plotted which guarantees better control of the sliding condition (Fig. 4),

- A dedicated system based on a ball bearing adjustment allows a single pad contact configuration to be implemented. The dispersion induced by contact misalignment and friction dispersion is reduced because only one contact needs to be adjusted. Besides, unlike to the symmetrical configuration which requires a complex finite plate thickness correction, the whole specimen thickness can be considered for the stress analysis, which justifies the semi-infinite contact hypothesis.

- This fretting fatigue setup enables the application of a negative loading ratio. In the present investigation, all the tests were performed for alternated fatigue loading conditions (R=-1).

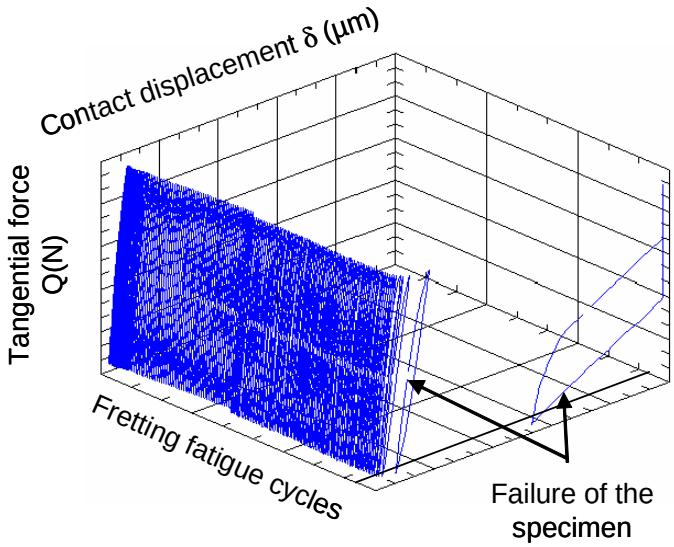

Fig. 4 : Typical Partial Slip Fretting Fatigue Log (i.e. plotting of the fretting cycles Q=f(δ) versus the fretting cycles (log scale) : When a crack is propagating the contact compliance is modified, shifting and altering the fretting cycle.

2.4. Identification of the friction coefficient at the sliding transition

Stress analysis of a fretting contact is highly dependent on the applied friction coefficient. Different approaches have been developed to determine this value [3, 19, 20]. A recent study shows that the friction coefficient measured at the transition between partial and gross slip conditions (μ_t) may be used to provide a representative value of the friction under partial slip conditions (i.e. $\mu_{PS} \approx \mu_t$) [21]. To determine the sliding transition of the studied contact, a variable displacement method was used: the normal load is kept constant while the relative displacement amplitude (δ^*) is progressively increased. For a 2D cylinder/plane configuration the sliding transition is marked by a discontinuity of the friction energy presently normalized through the energy ratio $A = E_d/E_t$, where E_d is the friction energy dissipated during the cycle, and $E_t = 4.Ft.\delta^*$ the total energy (i.e. the friction work done [19], Fig. 5). Several tests were performed for the studied pressure condition suggesting $\mu_t = 0.85 \pm 0.05$ may be taken as representative of the stabilized AISI 1034 / 52100 partial slip friction coefficient.

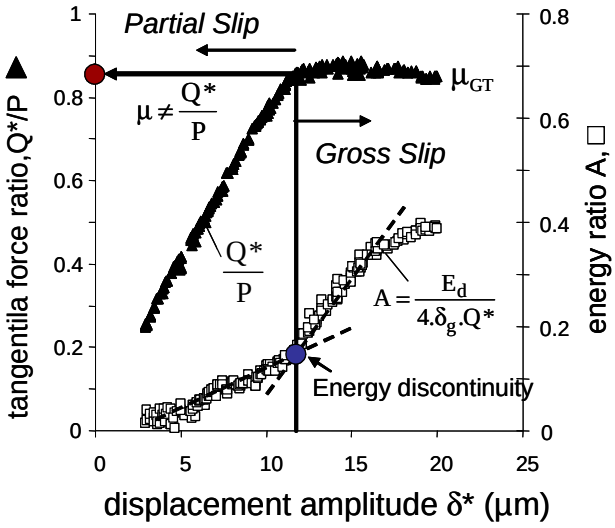

Fig. 5 : Illustration of the variable displacement method applied to the studied contact conditions. Ratio Q/P is increased until a stabilized gross slip condition is just reached. The energy ratio A is computed and exhibits a discontinuity at the transition.*

3. Stress field analysis

The studied pressure condition is quite high compared to the yield stress of the material (p_{0H} /σy=1.28). If a full sliding configuration is assumed, the very high friction coefficient will promote a generalized plastic deformation within the interface. However, because very small partial slip conditions are imposed, the plasticity is in fact constrained in narrow domains localized on the top surface sliding domains. Expecting that plasticity will have a minor impact, we assume an elastic description of the contact and subsurface stress field distribution. The elastic assumption is justified by considering the following aspects:

- Gros et al show that the AISI 1034 alloy displays a very high cyclic strain hardening behavior. Therefore after few cycles inducing plasticity, the material converges towards elastic shakedown,
- compared to the Hertzian prediction, the contact extension after the fretting test remains smaller than 7%. It indirectly supports the idea that plasticity is very localized and has a minor effect on pressure and shear stress field distributions,
- our analysis focuses on high cycle cracking damage (i.e. detection of crack nucleation limit above 10^6cycles). It is widely accepted that for such conditions, plasticity has a minor effect, at least at the macro scale description,
- our main objective is to provide a conservative prediction of fretting-fatigue damage. An elastic description overestimates the stress and therefore supports our pessimistic but safe damage tolerance strategy.

3.1. Plain fretting condition

The specimen thickness T=12 mm is defined so that each solid could be considered as an elastic half space, and hence the solution for the pressure distribution is Hertzian [16, 22]. Similarly, the subsequent application of an alternating tangential force gives rise to a symmetric shear traction distribution that is similar to that described by Mindlin and Deresciewicz [23]. A central stick zone ($|X| < c$) is bordered by regions of microslip (Fig. 6a). The contact half width, a, is small compared with the specimen thickness, T, (a/T ≈ 0.05) so that no thickness correction [23] is needed.

The contact pressure contribution is assumed to be constant and static due to the very small displacement amplitude:

$$p(x)/a = \sqrt{1-(x/a)^2} \qquad (1)$$

The description of the cyclic shear contribution is more complex, defined as the superposition of different elliptic distributions to describe the pulsing evolution of the sliding front from the external contact border (a) to the inner stick boundary (c) where:

$$c = a \cdot \sqrt{1 - Q^*/(\mu.P)} \qquad (2)$$

Hence, symmetrical shear stress field distributions are alternately imposed at the tangential force amplitudes +Q and –Q*.

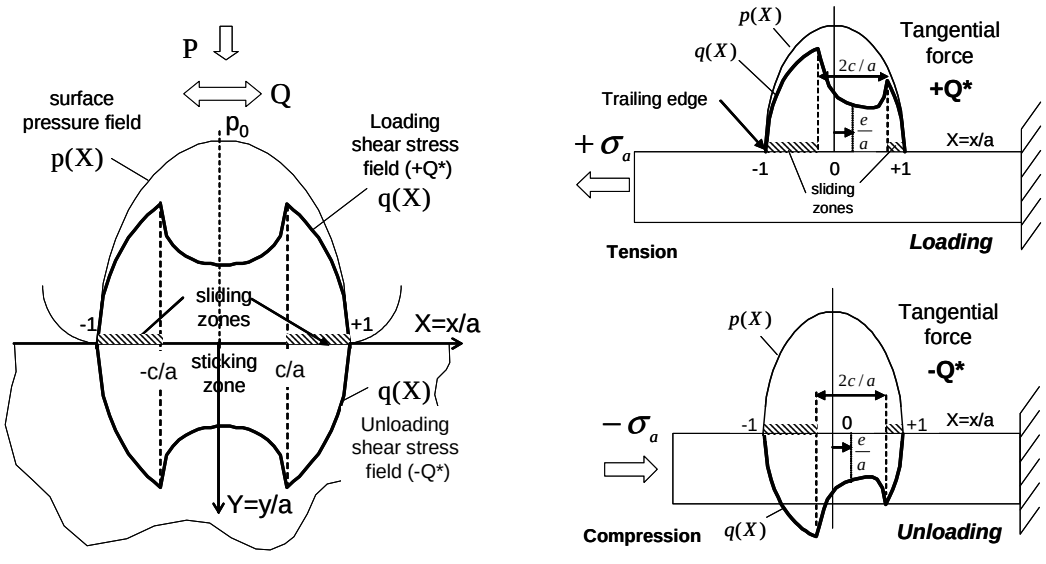

(a) (b)

Fig. 6 : Illustration of the pressure and shear stress field distributions : (a) plain fretting condition; (b) Fretting-Fatigue condition : Loading ($\sigma_{FATIGUE} = \sigma_a \Rightarrow Q = +Q^*$), Unloading ($\sigma_{FATIGUE} = -\sigma_a \Rightarrow Q = -Q^*$).

3.2. Fretting Fatigue loading conditions

The elastic Fretting Fatigue stress description is developed using an on phase Fretting - Fatigue loading condition. As shown by D. Nowell and al. [24], the bulk loading which is present in the fatigue specimen but not in the pad specimen promotes a mismatch in strains, causing an additional term in the tangential matching. The result of the couple effect of fatigue loading on the partial fretting contact stress is the introduction of an "e" offset of the centre of the sticking zone from the centre of the contact. For the specific condition where e+c≤a, an explicit expression of the offset is available:

$$e = \frac{\sigma \cdot a}{4 \cdot \mu \cdot p_0} \qquad (3)$$

Again, symmetrical shear stress field distributions are alternately imposed at tangential force amplitudes +Q and –Q* depending on the imposed bulk loading.

By contrast to the plain fretting condition, the dissymmetry of the sliding distributions promotes a larger sliding domain at the trailing edge of the contact (Fig. 6b).

If larger bulk stresses are applied, (i.e. e+c > a), reverse slip take place at one edge of the contact. Complex integral equations must then be solved to extract the shear stress field distribution.

Both fretting and fatigue loading are in phase and related to an alternating loading condition (stress ratio R=-1). The stress loading path can therefore be expressed by the two amplitude states, respectively, the so called loading and unloading conditions respectively (Fig. 8):

$$\Sigma_{loading} = \Sigma_{contact}(P,+Q^*) + \sigma_a$$

and

$$\Sigma_{unloading} = \Sigma_{contact}(P,-Q^*) - \sigma_a \qquad (4)$$

The maximum loading state conditioning the crack nucleation risk and the crack propagation is located at the trailing edge (X=-1) at the loading condition.

3.3. Estimation of subsurface stresses induced by the contact loading

When the size of the contacting bodies is large compared to the contact size, a good approximation might be to consider each body as an elastic half-plane. With this approximation, once the surface stresses are known, the subsurface stresses induced by the contact loadings can be found by superposing half- plane Green's functions. For example, a

general pressure distribution may be approximated in a piecewise-linear fashion by overlapping triangular elements as shown in Figure 7.

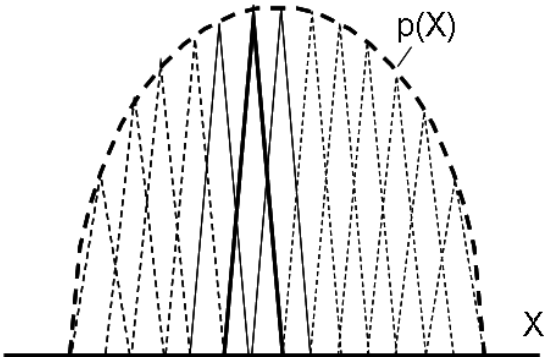

Fig. 7 : Illustration of influence function principles applied to plane contacts (piecewise linear) : application to the elliptical pressure distribution.

The stresses at any general subsurface point for an individual element are provided by Johnson in [16] either for pressure or shear components. Thus, the full stress field due to a general stress distribution may be obtained from appropriate superposition of the simplified expressions mentioned. The full details of this numerical procedure and the limits of its application are provided by K. L Johnson [16] and D.A. Hills et al. in [22]. To reproduce as closely as possible the complex pressure and shear stress fields derived from the above interface analysis, the total number of increments is presently increased up to 2000, providing a lateral resolution equivalent to 1/1000 of the half contact width (i.e. triangular width of about 0.32 µm).

4. Quantification of the crack nucleation risk

4.1. Crossland's Multiaxial Fatigue Criterion

To predict the Fretting-Fatigue crack nucleation risk at the fatigue limit condition (i.e. 10^6 cycles), the Crossland's multiaxial fatigue description is applied [25]. The crack risk is expressed as a linear combination of the maximum amplitude of the second invariant of the stress deviator ($\sqrt{J_2(t)}$) defined by ξ_a, and the maximum value of the hydrostatic pressure ($P_{h\,max}$).

The non cracking condition is expressed by :

$$\xi_a + \alpha_C \cdot P_{h\,max} < \tau_d \qquad (5)$$

Where

$$P_{h\,max} = \max_{t\in T}\left(\frac{1}{3}\,\mathrm{trace}(\Sigma(t))\right) \tag{6}$$

$$\xi_a = \frac{1}{2}\max_{t_0\in T}\left\{\max_{t\in T}\left[\frac{1}{2}\left(S(t)-S(t_0)\right):\left(S(t)-S(t_0)\right)\right]^{1/2}\right\} \tag{7}$$

$$\alpha_C = \frac{\tau_d - \sigma_d/\sqrt{3}}{\sigma_d/3} \tag{8}$$

with,

S : deviatoric part of Σ

σ_d : alternating bending fatigue limit,

τ_d : alternating shear fatigue limit.

The cracking risk can then be quantified through a scalar variable:

$$d_C = \frac{\xi_a}{\tau_d - \alpha_C \cdot P_{h\,max}} \tag{9}$$

The cracking condition is then expressed as:

- If d_C is greater than or equal to 1, there is a risk of cracking;

- If d_C remains less than 1, there is no risk of cracking.

4.2 Calibrating the crack nucleation prediction on plain fretting conditions

The first step of the methodology is to calibrate the model by iterating the experimental crack nucleation limit defined from plain fretting tests. To identify the experimental crack nucleation threshold, the following procedure is applied:

Keeping the pressure and the test duration constant, various tests are performed at different tangential force amplitudes. In the present investigation we focus on high cycle endurance conditions so we consider that the crack nucleation limit is reached at 10^6 cycles. Cross-sections at different places along the median axis of the fretting scars are then taken. The maximum crack lengths observed are plotted versus the applied tangential force amplitude (Fig. 8, Table 2). A linear approximation can be considered so that, the crack nucleation condition Q^*_{CN}, below which no crack can be observed can be extrapolated (i.e. b=0). For the studied condition we determine Q^*_{CN} = 100 N/mm (Fig. 8). Note that the crack nucleation condition is usually defined for an arbitrary crack length. Depending on the crack length, different crack nucleation thresholds might be considered. This paradox has been resolved by

defining the crack nucleation threshold as the limit stress condition below which no crack can be observed (b=0).

Table 2 : Evolution of the experimental crack length under plain fretting conditions as a function of the tangential force amplitude (10^6 cycles, p_{0H} = 450 MPa, a_H= 320 µm).

Tangential force amplitude Q* [N/mm] (R=-1)	90	98	126	137	144	146.0	151	164	169
Longest crack length observed b(µm)	0	0	24	29	31	51	55	64	68

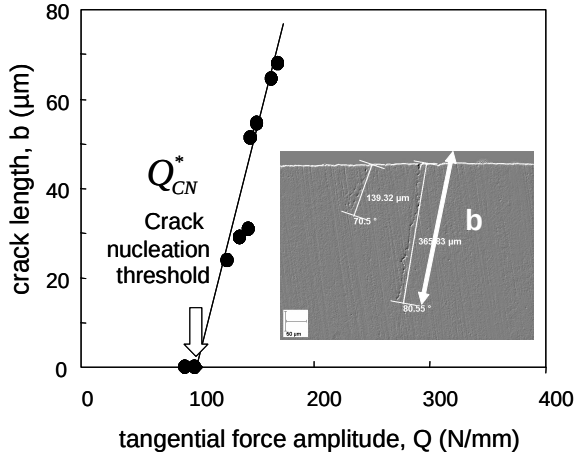

Fig. 8 : Experimental identification of the threshold tangential force amplitude(Q^*_{CN}) inducing a crack under plain fretting loading (10^6 cycles, p_{0H} = 450 MPa, a_H= 320 µm).

The multiaxial fatigue analysis is then performed for the threshold crack nucleation condition. Confirming the experiments, figure 9 shows that the maximum crack risk is located at the contact borders but the computed value d_C is around 2.

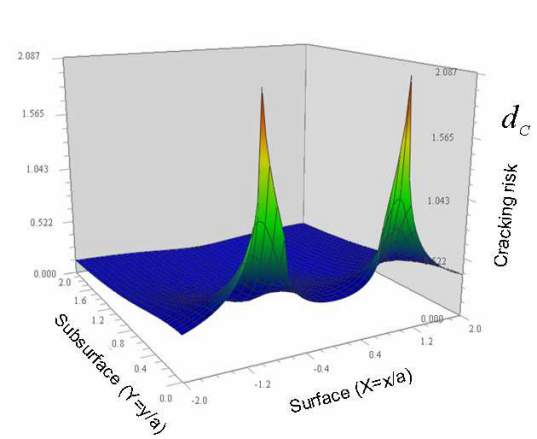

Fig. 9 : Illustration of the cracking risk below the interface under plain fretting conditions at the threshold crack nucleation condition (p_{0H} = 450 MPa, a_H= 320 µm, μ_t=0.85, Q^*_{CN} = 100 N/mm) defined from the Crossland criterion.

As mentioned previously, the current point stress analysis critically over-estimates the cracking risk.Indeed, the cracking risk analysis under severe stress gradient conditions requires to consider more representative loading condition averaging for instance le stress state over a representative length scale [6, 7]. A pertinent cracking risk analysis will consist first to identify a representative stress state taking into account the stress gradient (Σ_R) then to apply a multiaxial fatigue analysis. Taylor et al. [26] have extensively investigated such aspect focusing on the peculiar stress gradient generated by notch discontinuities but considering a crack propagation approach. We adopt the Taylor strategy, considering a multidimensional strategy to identify representative stress states but considering a multiaxial fatigue criteria analysis (Fig. 10).

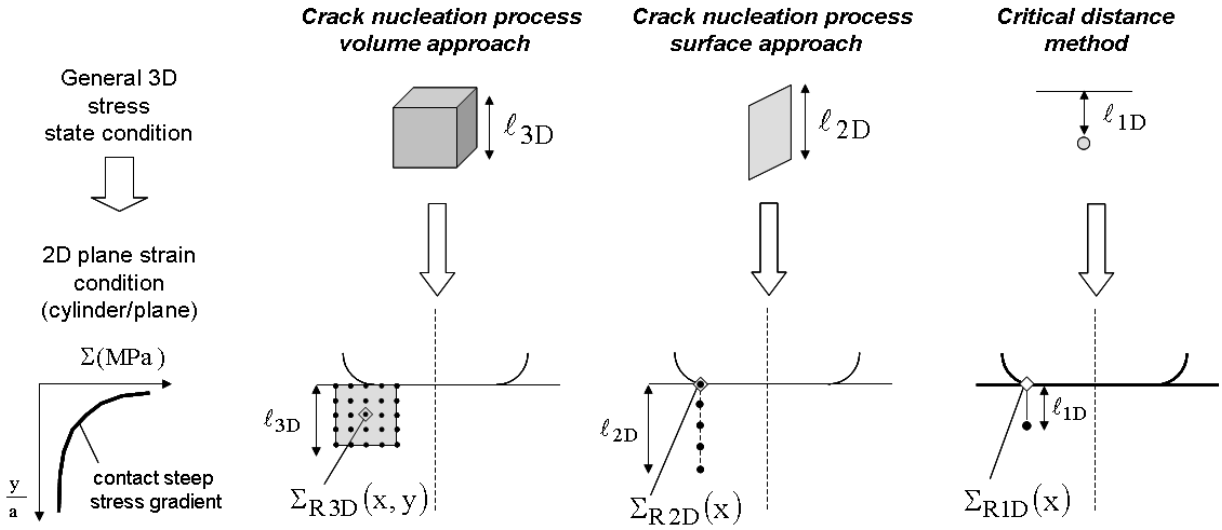

Fig. 10: Illustration of the length scale approaches applied to integrate the stress gradient effect; ◇ : point where is established the representative stress state; ● : point where is computed the stress state.

Crack nucleation process volume (3D averaging approach)

First introduced in Fretting problems [6], it consists to establish a representative loading state by averaging the stress state over a 3D representative "crack nucleation process volume". The point stress analysis is replaced by a mean loading state $\overline{\Sigma}(M)$ averaged over the micro volume V(M) surrounding the point on which the fatigue analysis is performed (M (x,y)) (Fig. 10) [6]. This micro volume of matter is approximated through a cubic volume, whose edges are assimilated to the physical length scale 'ℓ_{3D}'. For the studied 2D plain strain

configuration, the volume stress state analysis is reduced to a surface area averaging. The "3D" representative stress state is therefore expressed through the following expression:

$$\Sigma_{R3D}(x,y) = \overline{\Sigma}(V(M(x,y),\ell_{3D})) = \frac{1}{25}\cdot\sum_{i,j=-2}^{2}\Sigma(M(x+i\cdot\frac{\ell_{3D}}{4}, y+j\cdot\frac{\ell_{3D}}{4})) \quad (10)$$

Crack nucleation process surface (2D averaging approach)

A crack displays a planar morphology so there is a physical justification to consider a plane averaging procedure rather than a volume approach. Indeed, although it is simpler to implement, a volume averaging procedure involves out plane stress components and therefore can induce discrepancy. The "2D" representative stress state can be approximated by the mean loading state averaged over a square area, whose edges are assimilated to the physical length "ℓ_{2D}". In fretting fatigue problems crack nucleates at the surface trailing edge of the contact and usually propagates perpendicularly to the fatigue loading. The square area can therefore be assumed normal to the surface and the fatigue directions with one edge located on the top surface. For the studied 2D plain strain configuration, the analysis is reduced to a "y" line averaging procedure (Fig. 10).

The following formulation is thus considered:

$$\Sigma_{R2D}(x) = \overline{\Sigma}(L(M(x,y=0),\ell_{2D})) = \frac{1}{5}\cdot\sum_{i=0}^{4}\Sigma(M(x,i\cdot\frac{\ell_{2D}}{4})) \quad (11)$$

Critical distance method

This latter method is equivalent to the point stress analysis and do not involve an averaging procedure. However, rather than consider the surface stress discontinuity to predict the cracking risk, the fatigue analysis is performed from a stress state defined below the surface at a critical distance so called "ℓ_{1D}" . Like for the averaging procedures this infers a significant reduction of the maximum loading state and therefore a better integration of the stress gradient effect. For the studied 2D cylinder plane configuration the surface representative stress state related to the contact surface is expressed by the following expression:

$$\Sigma_{R1D}(x) = \Sigma(M(x,y=\ell_{1D})) \quad (12)$$

Different methodologies can be applied to extrapolate the former length scale parameters. Some approaches consider the crack length marking the transition from short to long crack propagation regime others are based on the grain size dimension. In the present investigation we adopt a reverse identification methodology involving iterative procedures to extrapolate

the optimized length values predicting the experimental plain fretting crack nucleation condition (i.e. p_{0H} = 450 MPa, a_H= 320 µm, μ_t=0.85, Q^*_{CN} = 100 N/mm). Figure 11 illustrates this methodology by plotting the evolution of the predicted cracking risk as a function of the 3D length scale parameter (i.e. process volume approach). A pertinent prediction of the cracking risk is found for ℓ_{3D} = 45 µm. This dimension is very close to the austenite grain size, which tends to confirm the hypothesis of a direct correlation between the length scale parameter and the microstructure [6]. The reverse identification methodology is then applied to identify the length scale parameters related to the crack nucleation process surface and the critical distance methods. We determine ℓ_{2D} = 55 µm and ℓ_{1D} = 20 µm respectively.

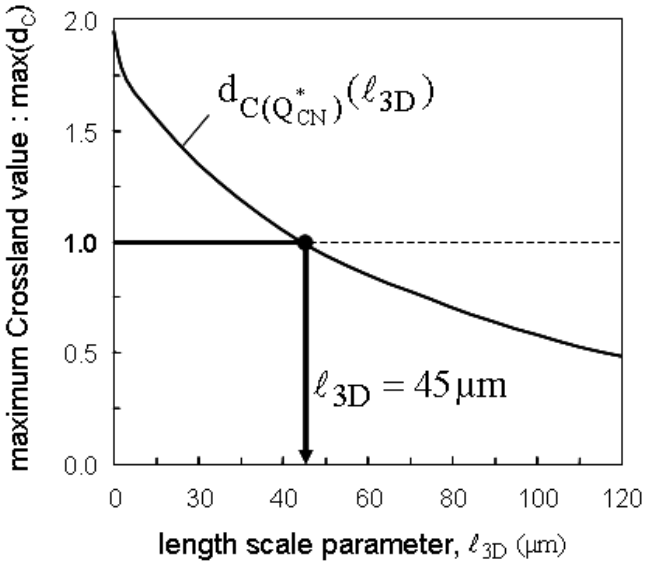

Fig. 11 : Illustration of the reverse identification approach to identify the representative length scale variable related to the crack nucleation process volume approach (ℓ_{3D}) from the plain fretting experiment (Q= Q^*_{CN}).*

4.3. Predicting the crack nucleation risk under Fretting-Fatigue loading conditions

To establish the experimental crack nucleation boundary under Fretting-Fatigue conditions, the following methodology has been applied. Three fatigue stress levels have been defined. For each fatigue level, different tests have been performed, adjusting the fretting tangential force amplitude by monitoring the test apparatus stiffness. Like for plain fretting investigations, the test duration was fixed at 10^6 cycles. After the test, cross section observations were performed to see if any cracks have been activated. The studied loading conditions are compiled in table 3.

Table 3: Studied Fretting Fatigue test conditions.

Fretting Fatigue Test (10^6 cycles)	Fatigue stress amplitude : σ_a [MPa] (R=-1)	Tangential force amplitude Q* [N/mm] (R=-1)	Cross section Examination
FF1	50	92	CRACK
FF2	50	82	NO CRACK
FF3	100	115	CRACK
FF4	100	110	CRACK
FF5	100	100	CRACK
FF6	100	80	NO CRACK
FF7	100	62	NO CRACK
FF8	120	91	CRACK
FF9	120	78	NO CRACK

Figure 12 plots the experimental damage as a function of the imposed fretting and fatigue loading conditions defining the so-called Crack Nucleation Fretting Fatigue Map (CN-FFM).

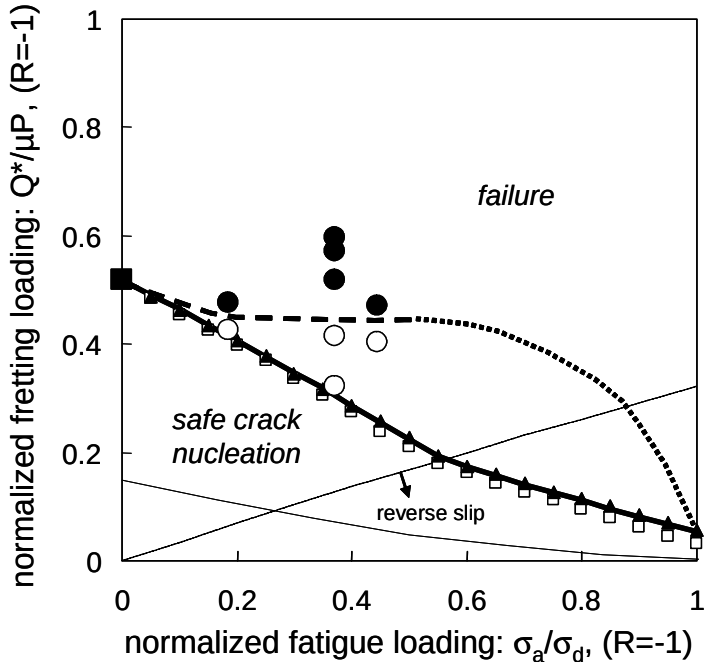

Fig. 12 : Illustration of the Crack Nucleation Fretting-Fatigue Map of AISI 1034 steel (p_{0H} = 450 MPa, a_H= 320 μm, μ_t=0.85, 10^6 cycles); ○ *no crack nucleation;* ● *crack nucleation;* ■ *crack nucleation threshold identified for plain fretting conditions;* ▬ ▬ ▪ *experimental crack nucleation boundary (▪▪▪▪▪▪▪▪ estimated evolution). Theoretical predictions (Crossland):* ____ *conventional point stress analysis;* ▬▬ *Crack nucleation process volume (ℓ_{3D} = 45 μm),* □ *Crack nucleation process surface (ℓ_{2D} = 55 μm);* ▲ *Critical distance method (ℓ_{1D} = 20 μm).*

The experimental crack nucleation boundary is estimated by separating both cracking and non cracking domains. It is characterized by an initial sharp decrease followed by a quasi constant evolution. Hence, the threshold crack nucleation boundary stabilizes at 80% of the plain

fretting condition in the middle fatigue stress range (i.e. σ_a/σ_d <0.5). The application of a fatigue bulk stress decreases the admissible fretting loading. However, its influence appears less determining than expected. This suggests that for the studied medium-low fatigue stress range (i.e. σ_a/σ_d <0.5), the crack nucleation process is mainly controlled by the contact loading. Further experiments are now required to investigate the crack nucleation process in the high fatigue stress region (i.e. $\sigma a/\sigma d$<0.5) in order to see until which fatigue stress condition the influence of the contact predominates and how the crack nucleation boundary converges toward the fatigue limit σ_a/σ_d =1).

To formalize the crack nucleation boundary, the multiaxial Crossland fatigue criterion is applied and the different length scale approaches compared. As expected, the conventional point stress analysis clearly underestimates the safe crack nucleation domain. It shows an asymptotic decrease from the plain fretting condition (i.e. $Q^*/\mu P$=0.18) to zero at the fatigue limit (i.e. σ_a/σ_d =1.0). This convergence toward a zero tangential loading is consistent with the fact that the stress state at the contact borders defined from the point stress methodology is dependent of the tangential force only. Therefore, when the bulk loading reaches the fatigue limit, the threshold tangential force amplitude is obviously equal to zero.

The length scale approaches (i.e. crack nucleation process volume, crack nucleation process surface and critical distance method), display quasi superimposed evolutions which suggests that, except numerical implementation considerations, none of them can be preferred to describe the stress gradient effect induced by fretting loading.

They shows a quasi linear decrease of the admissible tangential loading from the plain fretting condition down to a small residual positive value when σ_a/σ_d=1. This residual tangential force, estimated near $Q^*/\mu P$=0.05, is in fact required to compensate for the compressive stress state induced by the static normal component. Unlike the point stress analysis, the length scale approaches considers a loading region where the mean stress level controlled by the normal loading is not zero but compressive. This suggests that for low fretting and high fatigue loading conditions, crack nucleation could be observed outside the contact region. Such a peculiar situation was confirmed in different experimental investigations, and indirectly supports the applied length scale descriptions to quantify the crack nucleation risk under fretting fatigue conditions.

The length scale approaches are clearly more realistic than the conventional point stress to predict the safe crack nucleation domain. However the predictions are still uncertain:

- They provide a very good description of the crack nucleation process for the low fatigue stress range (i.e. σ_a/σ_d <0.1),

- Within the intermediate fatigue stress domain (i.e. $0.1<\sigma_a/\sigma_d<0.5$), the length scale approaches predicts a quasi-linear decrease of the crack nucleation boundary, whereas experiments conclude that the admissible fretting loading stabilizes. The higher the bulk stressing, the larger the discrepancy with the models.

- Convergence is however expected for the higher fatigue stress range ($0.5<\sigma_a/\sigma_d$ <1.0), which unfortunately can not be addressed in the present investigation.

The physical interpretation of this discrepancy is still an open question. The present investigation clearly demonstrates that it is not related to length scale numerical approach (i.e. applied averaging strategy). Alternative hypotheses must be considered, like plasticity which interacts with the stress distribution and introduces local residual stresses or the current length scale methods which is established from fixed length values but could be optimized by considering variable length scale dimensions as a function of the stress gradient fluctuations.

This underlines the necessity to establish fundamental research focusing on the latter aspects. However, one conclusion of this work is the fact that a multiaxial fatigue analysis combined with a length scale approaches calibrated from plain fretting conditions enables the crack nucleation risk under fretting fatigue loading conditions to be conservatively approximated.

Due to its capacity to be generalized for any stress configurations like subsurface stress discontinuities, the crack nucleation process volume approach will be preferred and applied in the following developments of this work.

5. Quantification of the crack propagation risk

5.1. Determining the Stress Intensity Factor (SIF)

Crack tip stress intensity factors have been found using the distributed dislocation method which is described in detail in [27]. The technique employs Bueckner's principle [28] which is simply an elastic superposition principle. Suppose a cracked body is subjected to the fretting fatigue load as depicted in Figure 13. A problem equivalent to the original would be the superposition of (A) and (B) where (A) represents the body without a crack subjected to the external fretting fatigue load and (B) a cracked body devoid of external loads but crack line traction and shear equal and opposite to the stress components along the line of the crack, so that after summing (A) and (B) the crack faces are traction free. Note that by taking this approach we are implicitly making the assumption that the effect of the crack on surface

displacements is small, so that surface stresses remain unchanged by the presence of the crack.

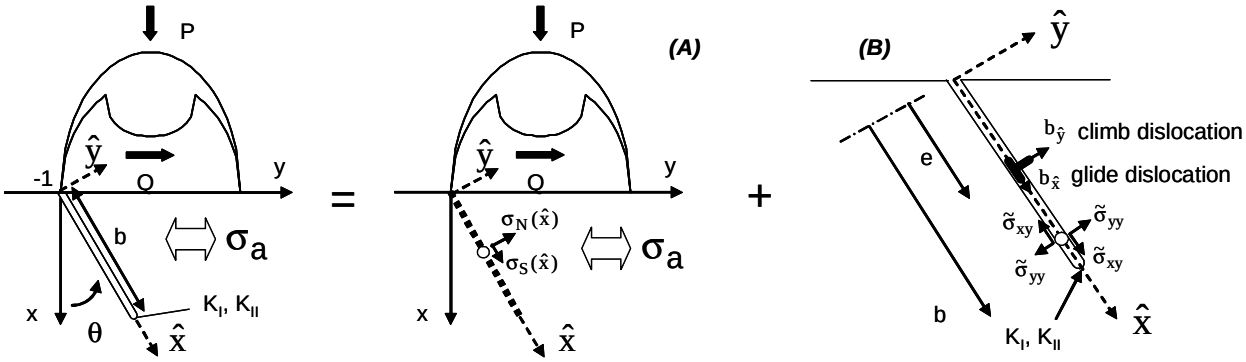

Fig. 13 : Bueckner's principle: (A) Body without crack subjected to contact load, (B) cracked body devoid of external loads but with crack line traction and shear equal and opposite to the crack line stress in (A). (Modified crack coordinates system defined from the (X, Y) contact system: x=Y/a; y=X/a-1).

Assuming the general case of a slant crack, a transformation of stress components is needed in order to determine the unsatisfied tractions (σ_N, σ_S) present along the crack faces. Since the crack faces have to be traction free, we distribute both climb and glide displacement discontinuities (or "dislocations") along the crack so that the stresses induced ($\tilde{\sigma}_{yy}, \tilde{\sigma}_{xy}$) cancel σ_N and σ_S. The integral equations expressing the requirement that the crack faces be traction free are:

$$\sigma_S(\hat{x}) + \frac{G}{4\pi(\nu+1)}\left\{\int_0^b B_{\hat{x}}(e)K_{\hat{x}}^S(\hat{x},e)\,de + \int_0^b B_{\hat{y}}(e)K_{\hat{y}}^S(\hat{x},e)\,de\right\} = 0$$

$$\sigma_N(\hat{x}) + \frac{2G}{4\pi(\nu+1)}\left\{\int_0^b B_{\hat{x}}(e)K_{\hat{x}}^N(\hat{x},e)\,de + \int_0^b B_{\hat{y}}(e)K_{\hat{y}}^N(\hat{x},e)\,de\right\} = 0 \qquad (13)$$

with G and ν the shear modulus and the Poisson coefficients.

Where $\sigma_S(\hat{x})$ and $\sigma_N(\hat{x})$ are the resolved shear and normal components of the stress tensor $\sigma(x,y)$ in the $(\hat{x},\hat{y})$ coordinate of the system, $K_{\hat{y}}^N$, $K_{\hat{x}}^S$, $K_{\hat{y}}^S$ are the kernels established by the above method detailed in [27, 29].

It is not possible to solve the equation analytically, but powerful numerical quadratures are given in references [27, 29]. The dislocation densities $B_{\hat{x}}$ and $B_{\hat{y}}$ are determined and the stress intensity factor K_I and K_{II} at the crack tip are successively approximated using a Krenk's interpolation [27]. Full details of the numerical procedure are given by Nowell and

Hills in [27]. We should recognize that the approach we have followed is purely elastic, whereas in practice some plasticity may be present.

5.2. Definition of an effective stress-intensity range parameter

A simplified single crack initiated at the contact trailing edge (X=x/a=-1), and normal to the surface (θ=0°) is considered. Note this assumption has been extensively considered in many Fretting-Fatigue investigations and was confirmed by examination of the cracking damage. Because pure alternating loading conditions are imposed (R=-1), the usual Elber's assumption that the effective mode I stress intensity range can be reduced to the maximum stress intensity value (i.e. $\Delta K_{Ieff} = K_{I\,max}$) is considered [13].

It has been shown that contact loading induces a mixed mode stress condition. Therefore the following hypotheses will be considered to quantify cracking behaviors:

A - Pure mode I

The mode II contribution is neglected and the effective stress intensity range is identical to the mode I component:

$$\Delta K_{eff\_A} = \Delta K_{Ieff} = K_{I\,max} \qquad (14)$$

where $K_{Im\,ax}$ is defined at the loading state (i.e. Q=+Q* and $\sigma_{FATIGUE}=+\sigma_a$).

B - Mixed mode neglecting the crack face friction

The mode II contribution is considered with the implicit assumption that crack face friction is negligeable (i.e. that mode II loading of the crack is unaffected by contact with the crack faces).

$$\Delta K_{eff\_B} = \sqrt{K_{Im\,ax}^2 + \Delta K_{IIeff}^2} \qquad (15)$$

$$\text{with } \Delta K_{IIeff} = K_{II\,max} - K_{II\,min} \qquad (16)$$

where $K_{II\,max}$ is defined at the loading state when $K_I = K_{Im\,ax}$ (i.e. open crack condition) and $K_{II\,min}$ computed at the unloading state (i.e. Q=-Q* and $\sigma_{FATIGUE}=-\sigma_a$, closed crack situation).

C - Mixed mode including the crack face friction

Many investigations confirm that friction phenomena within the crack interface reduce the mode II contribution. One approximation consists to neglect the mode II contribution when

the crack faces are under compression state (i.e. at the unloading state). The effective SIF range is therefore estimated by:

$$\Delta K_{eff\_C} = \sqrt{K_{Im\,ax}^2 + K_{II\,max}^2} \qquad (17)$$

5.3. Short crack methodology

The crack examination suggests that crack propagation may take place in the short crack regime when the actual stress intensity factor range is less than the long crack threshold, ΔK_0. We therefore intend to apply short crack approaches, to predict the crack arrest conditions. Two strategies are here considered. The first consists in a discontinuous description of the transition from short to long crack domains and the second, introduced by El Haddad and co-authors [12] considers a smooth continuous transition.

5.3.1 K-T's threshold of the short crack arrest condition

First introduced by Araujo et al. for fretting fatigue conditions [10], the starting point of this approximation is based on the Kitagawa and Takahashi diagram [11] which shows that many materials exhibit a long crack threshold which is independent of crack length. However, the K-T diagram also shows that cracks can propagate at $\Delta K < \Delta K_0$ provided that the stress is high enough. In a uniform stress field, such short crack behaviour may be interpreted as requiring that the applied stress range is greater than the establish fatigue limit σ_d. As a first approximation, the transition crack length (b_0) between short and long crack regimes can be extrapolated by equating these two conditions:

$$\Delta K_0 = 1.12 \cdot \sigma_d \cdot \sqrt{\pi \cdot b_0} \qquad (18)$$

hence,

$$b_0 = \frac{1}{\pi} \cdot \left(\frac{\Delta K_0}{1.12 \cdot \sigma_d} \right)^2 \qquad (19)$$

For the alloy used here, this gives b_0 = 170 µm (since ΔK_0 = 7 MPa√m). Following the approach adopted by Araújo et al. [10], we choose to examine the propagation of the crack in the *modified* K-T diagram (i.e. where ΔK rather than stress is plotted against *b*) (Fig. 14a) Hence, the threshold stress, ΔK_{th} is given by

$$\Delta K_{th} = \Delta K_0 \cdot \sqrt{\frac{b}{b_0}} \qquad b < b_0 \qquad (20)$$

$$\Delta K_{th} = \Delta K_0 \qquad b > b_0 \qquad (21)$$

Based on this description, the two quantities ΔK_0, and σ_d may be regarded as being the fundamental material properties needed to describe crack growth under both long and short crack regimes (Fig. 14a). The crack arrest condition is assumed when the following inequation is satisfied:

$$\Delta K_{eff} \leq \Delta K_{th} \; . \qquad (22)$$

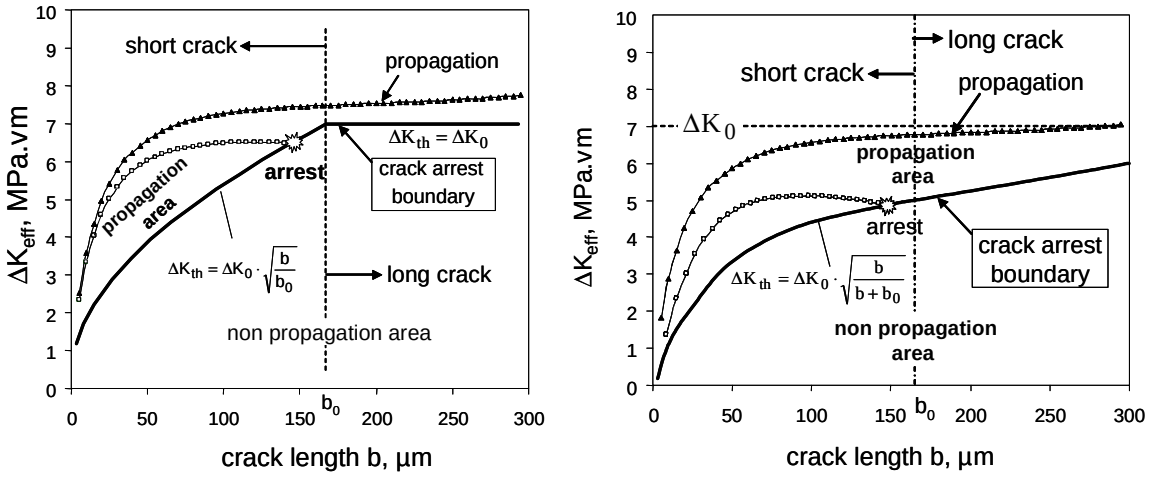

(a) (b)

Fig. 14 : Illustration of the short crack arrest methodology applied to predict crack propagation under fretting fatigue conditions after [10]) (For the studied steel, ΔK_0 = 7 MPa√m and b_0 = 170 µm): (a) K-T's approximation (discontinuous transition between short and long crack regime); (b) El Haddad's approximation (continuous transition between short and long crack regime).

5.3.2 El Haddad's threshold of the short crack arrest condition

Like for the previous description the transition from short to long crack behavior is related the threshold crack length b_0. However, rather than to consider a discontinuous transition we assume the continuous El Haddad's approximation of the short crack arrest threshold (Fig. 14b):

$$\Delta K_{th} = \Delta K_0 \cdot \sqrt{\frac{b}{b + b_0}} \qquad (23)$$

Fig. 14 confirms that whatever the crack length, the El Haddad's approximation will systematically provide a lower value of the threshold crack arrest condition. The difference is particularly important in the transition domain when b= b_0 . This suggests that the El Haddad's approximation is more conservative than the K-T's approach.

5.4. Predicting the crack arrest condition under Fretting-Fatigue loading conditions

To establish the experimental crack arrest boundary, the following methodology has been defined. Three levels of fretting loading have been selected, respectively $Q^*/\mu P$=0.5, 0.63 and 0.73. For each contact loading the alternated fatigue stressing has been adjusted from σ_a/σ_d= 0.4 to 0.6. The studied loading conditions selected above the crack nucleation boundary and the corresponding damage evolutions are reported in Table 4.

Table 4 : Studied Fretting Fatigue test conditions.

Fretting Fatigue Test (10^7 cycles)	Fatigue stress amplitude : σ_a [MPa] (R=-1)	Tangential force amplitude Q* [N/mm] (R=-1)	Maximum crack length expertised : b (µm)
FF10	120	145	344
FF11	120	125	290
FF12	120	100	59
FF13	130	145	broken
FF14	130	125	broken
FF15	130	100	broken
FF16	140	125	broken
FF17	150	125	broken
FF18	160	125	broken

By contrast to the nucleation phenomenon, propagation failure can be observed after several million cycles. Therefore, to estimate the stabilized crack arrest conditions the test duration was increased up to 10 million cycles. Hence, for each test, cracking damage is characterized by reporting either if the specimen is broken after 10^7 cycles or the maximum crack length found for unbroken specimens. All the experimental results are reported in Figure 15, defining the so-called Crack Arrest Fretting Fatigue Map (CA-FFM). Like for the crack nucleation analysis, the experimental crack arrest boundary can be extrapolated from failure and non failure conditions. The experimental crack arrest boundary displays a quasi vertical evolution, which suggests that the crack arrest process is only a function of the fatigue loading and relatively unaffected by the contact stress. This result, combined with the previous crack nucleation investigation, confirms the conventional idea that under fretting-fatigue, crack

nucleation is controlled by contact loading, whereas crack arrest is mainly controlled by fatigue bulk stressing. This conclusion is however restricted to the medium fatigue stress range ($0.4 < \sigma_a/\sigma_d < 0.6$) and must be tempered regarding the relative contact size.

To predict the crack arrest boundary the following methodology is applied:

The crack modeling was carried out assuming a single crack normal to the surface and located at the trailing edge (X=-1), where the maximum value of the crack nucleation risk has been found. Then for each fretting loading condition, the modeling strategy consists to identify by iterative computations, the maximum fatigue stressing below which the crack arrest condition is achieved.

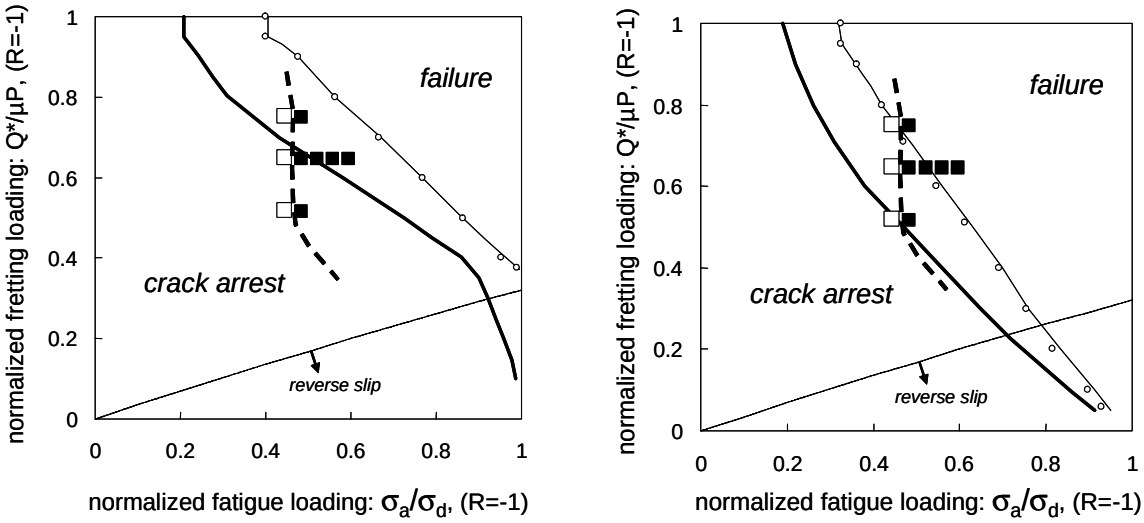

Fig. 15 : Illustration of the Crack Arrest Fretting-Fatigue Map of the AISI 1034 steel (p_{0H} = 450 MPa, a_H= 320 μm, μ_t=0.85, 10^7 cycles): ■ : broken specimen; □ : unbroken specimen; – – : experimental boundary defining the crack arrest condition; Theoretical prediction : (a) K-T's short crack arrest approximation, (b) El Haddad's short crack arrest approximation; —— : plain mode I approximation (ΔK_{eff_A}) ; ▬▬ : Mixed mode approximation (ΔK_{eff_B});○ Mixed mode including the crack face friction (ΔK_{eff_C}).

This analysis is applied for the different approximations of the effective SIF range parameters and the two short crack arrest approaches. It is interesting to note that the $K_{II\,max}$ value, defined at the loading condition (i.e. Q=+Q*, $\sigma_{FATIGUE}$=+σ_a), is negligible compared to the $K_{I\,max}$ variable. This permit to explain the quasi superimposition of the boundaries defined either considering a pure mode I contribution ($\Delta K_{eff\_A} = K_{I\,max}$) or assuming a mixed mode considering the crack face friction ($\Delta K_{eff\_C} = \sqrt{K_{Im\,ax}^2 + K_{II\,max}^2}$). In fact the

mode II contribution displays a maximum influence at the unloading state when Q=-Q*, $\sigma_{FATIGUE}=-\sigma_a$. This is confirmed by the large difference observed between the crack arrest boundaries defined from the mode I estimation and the conventional mixed mode approximation $\Delta K_{eff\_B} = \sqrt{K_{Im\,ax}^2 + \Delta K_{IIeff}^2}$. As previously suggested, the introduction of the mode II contribution ($\Delta K_{IIeff} \approx |K_{II\,min}|$), by providing a higher estimation of the effective SIF range, promotes more pessimistic estimations of the crack arrest condition and finally induces a reduction of the crack arrest domain.

The comparison between short crack arrest approximations confirms the El Haddad's description as the most physically and quantitatively reliable approach:

- By contrast to the K-T's approximation, which shows a discontinuous evolution for the highest fretting loadings, the El. Haddad's assumption provides a more realistic continuous evolution of the crack arrest boundary.
- Whatever the SIF approximation, the K-T's assumption systematically under estimates the crack propagation conditions, and promotes dangerous optimist estimation of the safe crack arrest situation. The El Haddad's description provides more conservative and realistic estimation of the crack arrest domain.

Combining the El' Haddad approximation and mixed mode estimation of the effective SIF range (ΔK_{eff_B}), a reliable and conservative prediction of experimental results is achieved. All the failure conditions are predicted. The model is even able to discriminate the non failure condition (FF12) from the failure situation (FF15) which are characterized by fatigue stress difference is less than 10 MPa.

This investigation also suggests that a plain mode I description and the K-T's approximation can induce dangerous optimistic crack arrest predictions. A significant discrepancy between the experimental crack arrest boundary and the safe El Haddad – mixed mode approximation is however still observed. This infers that more elaborated formulations, taking into account plasticity, closure and representative friction effects in the crack faces should be introduced in the model. Besides more complete short crack arrest descriptions, have to be considered for future optimization of the modeling. This complete description will however require an expensive in depth investigation of the studied material, which unfortunately was not possible in the framework of this research. However, the main objective of this work is to provide realistic and safe estimations of the cracking response. Therefore, in spite of its limitations, the current pessimist strategy which combines an El Haddad description of the short crack

arrest condition, an elastic description of the stress field and the application of a mixed-mode formulation appears to be a good compromise to approximate the crack arrest boundary in the CA-FFM initially.

6. Synthesis

Both crack nucleation and crack arrest boundaries are reported on the same graph defining the so call Fretting-Fatigue Map (Fig. 16). The experimental results are compared respectively with the model of crack nucleation defined from the Crossland's multiaxial fatigue criterion by taking into account the stress gradient effect through a 3D process volume description and, with the crack arrest boundary defined from the El Haddad-mixed mode approximation.

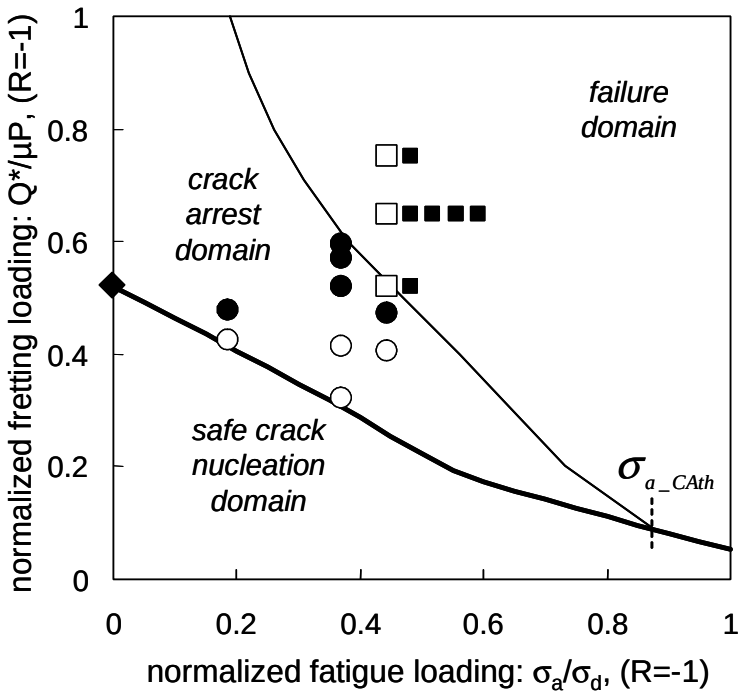

Figure 16 : Fretting-Fatique map of the AISI 1034 steel (p_{0H} = 450 MPa, a_H= 320 µm, μ_t=0.85): ○ : no crack nucleation (10^6 cycles); ● : crack nucleation (10^6 cycles); ◆ : crack nucleation threshold identified for plain fretting conditions (10^6 cycles); ■ : broken specimen (10^7 cycles); □ : unbroken specimen (10^7 cycles); ——— : theoretical crack nucleation boundary (Crossland, ℓ_{3D} = 45 µm) ; ——— : theoretical crack arrest boundary (El Haddad's-short crack arrest methodology using friction free mixed-mode approximation).

It is interesting to note that above a given bulk stress (σ_{a_CAth}), the so called Fretting – Fatigue crack arrest bulk stress limit, the crack arrest boundary passes below the crack nucleation boundary. Above this bulk stress limit, if a crack nucleates, it systematically

propagates until failure. The contact evolves directly from a safe non-crack nucleation situation to a catastrophic failure configuration.

This key loading point must be determined for optimized safe fretting fatigue designing:

Below σ_{a_CAth} , a two-threshold damage strategy can be considered. For the lowest contact conditions, a safe crack nucleation design can be considered. For higher fretting stress conditions, an alternative safe crack arrest approach is still applicable.

Above σ_{a_CAth} (i.e. for high fatigue stress), only a crack nucleation strategy can be considered.

The key point loading σ_{a_CAth} , is dependent on many factors such as the materials properties (i.e. elastic, plastic and fatigue properties), the normal loading, the contact geometry [30] and corresponding contact stress field distributions, the friction coefficient and numerous other aspects like environmental interactions etc …. Future investigations will focus on investigating the influence of each of these parameters.

However in the framework of this first description, it appears interesting to evaluate the relative impact of fatigue parameters like σ_d and ΔK_0. This analysis is illustrated by comparing the studied AISI 1034 to the prediction obtained for a Ti-6Al-4V alloy applying a similar methodology. The mechanical and fatigue properties of this alloy are compiled in table 1. A previous investigation performed for similar plain fretting conditions and applying the Crossland formulation extrapolates the crack nucleation length scale parameter near ℓ_{3D} = 35 µm. To isolate the relative influence of fatigue properties and provide a direct comparison between the fretting fatigue maps, the contact configuration has been adjusted to keep the maximum pressure p_{0H} =450 MPa, the contact dimension a_H= 320 µm and the fiction coefficient μ_t =0.85 constant. Note that such "contact" similitude can be achieved if the Ti-6Al-4V plane is pressed against a 30 mm radius 52100 cylinder steel cylinder with a same P=227 N/mm normal loading. The comparison is then given for similar stress ranges with the tangential force amplitude normalized by $P.\mu_t$ = 193 N/mm and the fatigue stress amplitude by the fatigue limit of the AISI 1034 steel ($\sigma_{d(AISI\,1034)}$ = 270 MPa).

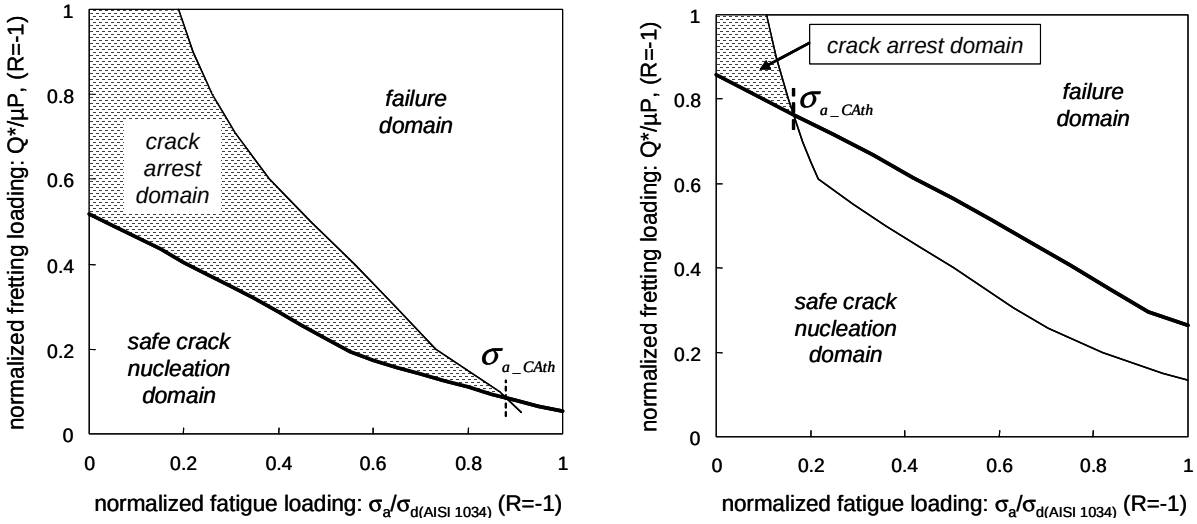

Figure 17 : Synthetic Fretting Fatigue Map; ——: theoretical crack nucleation boundary (Crossland) ; ——: theoretical crack arrest boundary using El Haddad short crack arrest methodology (mixed mode approximation) (P=227 N/mm, p_{0H} =450 MPa, a_H= 320 μm, μ_t =0.85) : (a) : AISI 1034/52100 (R=40 mm, ℓ_{3D} =45 μm); (b) Ti-6Al-4V/52100 (R=30 mm, ℓ_{3D} =35 μm).

The synthetic Fretting-Fatigue charts are compared in Figure 17. The Ti-4Al-6V alloy displays a significantly larger crack nucleation domain, although its length scale parameter ℓ_{3D} is smaller and therefore the stress discontinuity averaging is less effective. This is explained by the very high fatigue limit of the titanium alloy, nearly twice that of the AISI 1034 steel. The comparison also shows that the Ti-6Al-4V alloys display a very small crack arrest domain. The fatigue stress threshold σ_{a_CAth} is translated to a smaller value. The crack arrest is so small that the safe cracking domain is nearly reduced to the safe crack nucleation area. This is explained by the low ΔK_0 values characterizing the titanium alloy.

To rationalize the analysis, we introduce the KS ratio:

$$KS = \Delta K_0 / \sigma_d \qquad (19)$$

The values obtained for the AISI 1034 and the Ti-6Al-4V alloys are $KS_{(AISI1034)}$= 2.6 10^{-2} $\sqrt{m}$ and $KS_{(Ti\text{-}6Al\text{-}4V)}$=1.1 10^{-2} $\sqrt{m}$ respectively. Comparing the Fretting-Fatigue charts, it can be said that the higher the KS ratio, the larger the crack arrest domain compared to the safe crack nucleation region, and the larger the limit σ_{a_CAth} defining the domain where the crack arrest methodology can be applied.

This analysis is important from the practical point of view of optimizing material selection. If, for technical considerations, the contact stress is so severe that a crack nucleation will be

systematically activated, a reasonable strategy is to optimize the contact configuration to maintain a crack arrest situation while decreasing the applied bulk stress loading, and to select an alloy displaying the highest possible ΔK_0 value (i.e. high KS ratio).

By contrast, if the system is running under high bulk fatigue stressing conditions (i.e. $\sigma_a > \sigma_{a\_CAth}$), a safe crack nucleation strategy should be preferred, and the material selected should have the highest possible σ_d values (i.e. low KS ratio). It also suggests important conclusions concerning the safe Fretting Fatigue cracking designing procedures as a function of the applied materials.

In rail train applications where the AISI 1034 steel is widely used, the application of the crack nucleation approach for Fretting Fatigue configuration promote safe and pessimistic predictions of the cracking damage. Indeed, except for the highest fatigue stressing, the crack nucleation boundary is bordered by the crack arrest domain. Therefore even if a crack nucleates, the crack arrest mechanism will limit a catastrophic failure.

The conclusions are fully different for the Ti-6Al-4V alloy which is extensively applied in aeronautical industries. Except for the very low fatigue stress range, the crack arrest boundary is located below the crack nucleation boundary. This infers the following remarks:

The crack nucleation strategy which is extensively applied in the designing procedure must be considered with caution. Indeed, if a crack nucleates, no crack arrest mechanism can block the successive propagation stage.

A damage tolerance approach, based on a crack arrest methodology, appears more conservative than a conventional crack nucleation strategy and therefore should be preferred to compute safe fretting fatigue structures of such low ΔK_0 alloys.

In the previous paragraph it was discussed how the fatigue properties of the bulk material can interact on the cracking evolutions and the selection of pertinent damage designing procedures. However, in most fretting problems, surface palliatives are usually applied to reduce the cracking risk [32]. A first approach consists in drastically reducing the coefficient of friction and consequently the cyclic fretting stresses. However, in many assemblies, a medium friction value is in fact required either to fix the contact or to allow a given friction dissipation in order to avoid some catastrophic dynamical problems. Therefore, keeping constant the coefficient of friction, specific coatings can be applied to prevent the crack nucleation process. This can be achieved using thin hard coatings, like PVD TiN coating, which inducing very high and stable compressive stresses will definitively block the surface crack nucleation process (Fig. 18a). The crack nucleation can also be avoided by applying tick

soft coating like plasma CuNiIn layer. The top surface fretting stresses are fully accommodated by the plastic deformation of the layer and bulk material is then protected from the crack nucleation.

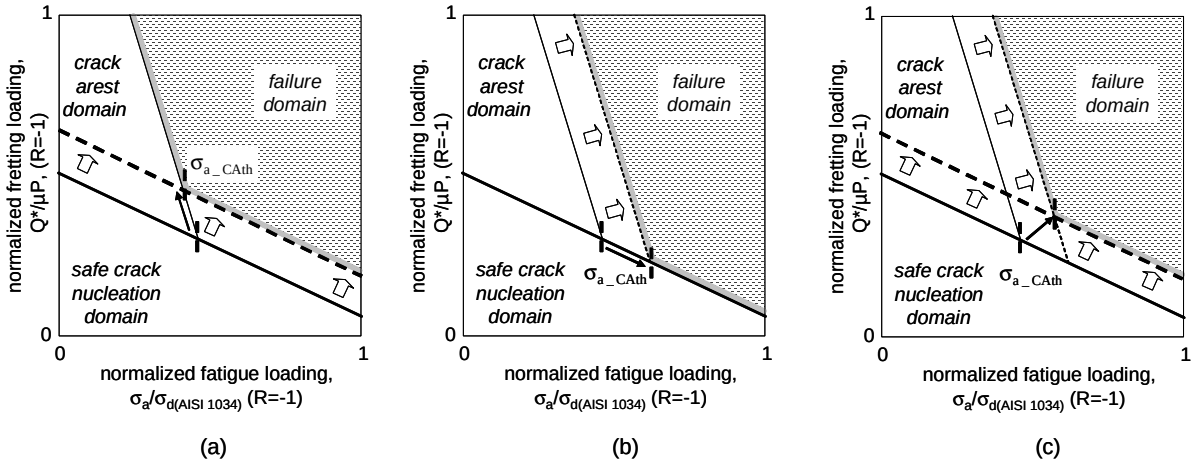

Fig. 18 : Illustration of the palliative strategy against fretting fatigue cracking : (a) Application of surface coating to extend the crack safe crack nucleation domain; (b) Application of an in depth surface treatment to extend the crack arrest domain; (c) Combined crack nucleation / crack arrest strategy (—— crack nucleation boundary, —— crack arrest boundary, —— ultimate safe cracking limit).

A second strategy consists to apply in depth surface treatment to limit and even block the crack propagation (Fig. 18b). Shot peened and laser peened are the most common treatments of such category. It consists to introduce compressive residual stresses deeper below the surface through the application of plastic deformations. By contrast to conversion treatments or thin hard coatings, these compressive stresses are not stable and, when a cyclic loading overpasses the plastic yield, the compressive residual stresses are partly or fully erased. Fretting loading tends to relax the surface compressive stresses and explains why it is usually admitted that shot peening treatment don't improve the crack nucleation response of fretting fatigue contact. However below the surface, where the contact stressing is becoming lower, the residual compressive stresses are maintained and will play a determining action to block the crack propagation.

For critical systems like dovetail contact of turbine engines these two palliative strategies are combined (Fig. 18c) either to extend the crack nucleation domain by applying thick soft coating like CuNiIn and Aluminium-bronze layers or to increase the crack propagation resistance by introducing very deep residual compressive stress field using shot peened and now laser peened. As illustrated by Figure 18, the given Fretting-Fatigue Mapping concept appears as a useful approach to quantify and compare the relative benefit of palliative strategies against fretting fatigue damages.

7. Conclusion

An experimental methodology has been developed to identify, respectively, crack nucleation and crack arrest conditions as a function of the applied fretting and fatigue loadings. Synthetic Fretting Fatigue maps have been introduced defining, respectively, the safe crack nucleation, crack arrest and catastrophic failure material responses. It is shown that a basic elastic approximation of the fretting-fatigue loading combined with a Crossland multiaxial fatigue analysis is able to predict the crack nucleation boundary if the contact stress gradient effect is taken into account. This can be achieved by considering a process volume methodology, where the stress state considered for the multiaxial fatigue analysis is averaged over a representative volume. Indeed, it was shown that for the peculiar stress gradient imposed by a contact fretting loading, the different stress averaging approaches like the 3D stress process volume, the 2D stress process surface and the critical distance method converge to similar results. This work shows that the process volume approach can be calibrated by using plain fretting tests, and extrapolated to more complex fretting fatigue configurations. It is also shown that a plain El Haddad's short crack arrest methodology combined with mixed mode SIF approximation allows a conservative description of the crack arrest domain. Based on these different approximations, Fretting Fatigue maps of different materials can be compared, assuming a "contact analog" description. To evaluate the relative influence of fatigue properties regarding the respective distribution of material response, the KS fatigue parameter, defined as the ratio between the long crack threshold ΔK_0 and the fatigue limit σ_d, is considered. A relative description of Fretting Fatigue Maps concludes that the higher the KS ratio, the larger the crack arrest domain, whereas the smaller the KS ratio the larger the safe crack nucleation area. Taking into account the material properties and the applied contact configuration, different safe damage designing can then be adopted, focusing either on crack arrest or safe crack nucleation strategies.

References

[1] Hoeppner DW, Chandrasekaran V, Elliot CB, editors. Fretting fatigue: current technology and practices; ASTM STP 1367, American Society for Testing and Materials, 2000, ISBN 0-8031-2851-7.

[2] Waterhouse, R.B., Fretting Fatigue, Applied Science publishers, 1981.

[3] Hills DA, Nowell D. Mechanics of fretting fatigue, Dordrecht: Kluwer Academic Publishers, 1994.

[4] Fouvry S., Kapsa Ph., Vincent L., Dang Van K. Theoretical analysis of fatigue cracking under dry friction for fretting loading conditions. Wear 1996;195:21-34.

[5] Szolwinski, M.P., Farris, T.N. Mechanics of fretting crack formation. Wear 1996;198: 93-107.

[6] Fouvry S, Kapsa Ph, Sidoroff F, Vincent L Identification of the characteristic length scale for fatigue cracking in fretting contacts. J. Phys. IV France 1998; 8: 159-166.

[7] Araújo JA, Nowell D. The effect of rapidly varying contact stress fields on fretting fatigue. International Journal of Fatigue 2002; 24 (7): 763-775.

[8] Giannakopoulos AE, Lindley TC, Suresh S, Chenut C. Similarities of stress concentrations in contact at round punches and fatigue in notches: implications to fretting fatigue crack initiation. Fatigue and Fracture of Engineering Materials and Structures 2000;23:562–71.

[9] Mugadu A, Hills DA, Barber JR, Sackfield A. The application of asymptotic solutions to characterising the process zone in almost complete frictional contacts. International Journal of Solids and Structures 2004; 41 (2):385-397.

[10] Araújo JA, Nowell D. Analysis of pad size effects in fretting fatigue using short crack arrest methodology, International Journal of Fatigue 1999;21:947-956.

[11] Kitagawa H, Takahashi S. Application of fracture mechanics to very small cracks or the cracks in the early stage. Philadelphia: American Society for Metals, 1976:627-630.

[12] El Haddad MH, Smith KN, Topper TH. Fatigue crack propagation of short cracks. Journal of Engineering Materials and Technology 1979;101:42-46.

[13] Gros V. Etude de l'amorçage et de la propagation des fissures de fatigue dans les essieux-axes ferroviaires, D. Phil. Thesis, Ecole Centrale de Paris, France,1996.

[14] Fouvry S, Duo P, Perruchaut Ph. A quantitative approach of Ti-6Al-4V fretting damage: Friction, Wear and crack nucleation. Wear 2004; 257(9-10): 916-929.

[15] Nicolas T., High Cycle Fatigue: A mechanics of materials perspective, Elsevier Eds, 2006.

[16] Johnson KL., Contact Mechanics, Cambridge University Press,1985.

[17] Zhou Z. R., Vincent L. Mixed fretting regime. Wear 1995;181-183(2):531-536.

[18] Kubiak K., Fouvry S., Marechal A.M., Vernet J.M. Behaviour of shot peening combined with WC–Co HVOF coating under complex fretting wear and fretting fatigue loading conditions. Surface and Coatings Technology 2006; 201(7):4323-4328.

[19] Fouvry S., Kapsa Ph., Vincent L. Developments of fretting sliding criteria to quantify the local friction coefficient evolution under partial slip condition. Tribology Series1998; 34:161-172.

[20] Dini, D. Nowell D. Prediction of the slip zone friction coefficient in flat and rounded contact Wear. 2003;254 (3-4):64-369.

[21] Proudhon H., Fouvry S., Buffière J.-Y. A fretting crack initiation prediction taking into account the surface roughness and the crack nucleation process volume. International Journal of Fatigue,2005; 27(5):569-579.

[22] Hills, D.A., Nowell, D., Sackfield, A. Mechanics of Elastic Contacts, Oxford Butterworth- Heinemann , 1993.

[23] Mindlin RD, Deresciewicz H. Elastic sphere in contact under varying oblique forces. J Appl Mech 1953, 75:327-344.

[24] Nowell, D., Hills, D.A., Mechanics of Fretting Fatigue tests. Int. Jnl. Mech. Sci. 1987;29(5):355-365.

[25] Crossland B. Effect of large hydrostatic pressures on the torsional fatigue strength of an alloy steel. Proceeding of the Inter. Conf. On Fatigue of Metals, Inst. of Mechanical Engineers, London, 1956, pp. 138-149.

[26] Taylor D., Geometrical effects in fatigue: a unifying theoretical model. International Journal of Fatigue 1999; 21:413-420.

[27] Nowell D, Hills DA. Open cracks at or near free edges. J Strain Analysis 1987; 22 (3): 177-185.

[28] Bueckner HF. The propagation of cracks and the energy of elastic deformation. Trans ASME 1958; 80:1225-1230.

[29] Hills D. A., Kelly P.A., Dai D.N., Korsunsky A.M., Solution of Crack Problems: The distributed dislocation technique, Kluwer Academic Publishers, 1996.

[30] Fouvry S., Nowell D., Kubiak K., Hills D.A. Prediction of fretting crack propagation based on a short crack methodology. Engineering Fracture Mechanics 2008; 75 (6):1605-1622.

[31] Nowell D., Dini D., Hills D.A. Recent developments in the understanding of fretting fatigue. Engineering Fracture Mechanics 2006;73(2):207-222.

[32] S. Fouvry, V. Fridrici, C. Langlade, Ph. Kapsa, L. Vincent, Palliatives in Fretting : A dynamical approach, Tribology International 2006;39:1005–1015.